Nanoscale

ROYAL SOCIETY OF CHEMISTRY

PAPER

View Article Online
View Journal | View Issue

Cite this: *Nanoscale*, 2024, **16**, 3160

Observation of different Li intercalation states and local doping in epitaxial mono- and bilayer graphene on SiC(0001)†

Wei Huang, Jeong Ah Seo, Mark P. Canavan, Pietro Gambardella and Sebastian Stepanow *

Received 26th June 2023,
Accepted 10th January 2024

DOI: 10.1039/d3nr03070a

rsc.li/nanoscale

Li intercalation is commonly used to enhance the carrier density in epitaxial graphene and mitigate coupling to the substrate. So far, the understanding of the intercalation process, particularly how Li penetrates different layers above the substrate, and its impact on electron transport remains incomplete. Here, we report different phases of Li intercalation and their kinetic processes in epitaxial mono- and bilayer graphene grown on SiC. The distinct doping effects of each intercalation phase are characterized using scanning tunneling spectroscopy. Furthermore, changes in the local conduction regimes are directly mapped by scanning tunneling potentiometry and attributed to different charge transfer states of the intercalated Li. The stable intercalation marked by the formation of Li–Si bonds leads to a significant 56% reduction in sheet resistance of the resulting quasi-free bilayer graphene, as compared to the pristine monolayer graphene.

1. Introduction

Epitaxial graphene prepared on Si-terminated SiC surfaces offers large-scale production and integration in devices, such as graphene field-effect transistors.[1] During the growth process of graphene by thermal decomposition of SiC, a carbon buffer layer forms first, and Si dangling bonds are left in the SiC substrate. Monolayer (MLG) or bilayer graphene (BLG) grows further on the buffer layer depending on the temperature or pressure.[2,3] However, the SiC substrate induces an intrinsic electron doping, which strongly pins the graphene's Fermi level to 0.4 eV above the Dirac point.[4,5] Following the idea of chemical doping for semiconductors, the intercalation of atomic species beneath graphene provides a viable route to separate the buffer layer from the substrate and shift the doping level from p-type to n-type or near charge neutrality. By utilizing specific intercalants, graphene can gain unique features, including increased spin–orbit coupling, superconductivity, and spin polarization.[6–8] Li intercalation is of great interest since it can largely increase the carrier density and generate clean quasi-free graphene with its out-of-plane orbitals undisturbed.[9] Furthermore, more carriers in graphene lead to stronger electron–phonon coupling causing superconductivity[10,11] or the Kekulé order through enhanced many-body interactions.[12]

Previous X-ray photoelectron spectroscopy (XPS) and low-energy electron diffraction (LEED) measurements have shown that Li atoms can penetrate through graphene layers directly and detach the buffer layer *via* bonding to Si at room temperature.[13] A new superstructure pattern $(\sqrt{3} \times \sqrt{3})R30°$ has been observed after the deposition, which is similar to the bulk C_6LiC_6 structure and disappears after heating at around 325 °C. Scanning tunneling microscopy (STM) imaging of the Li intercalated MLG shows that Li nucleation starts at the SiC steps and then grows inwards.[14] Further scanning tunneling spectroscopy (STS) measurements reveal n-doping corresponding to a 0.8 eV shift of the charge neutrality point, which agrees with observations from angle-resolved photoemission spectroscopy.[13,15] An even higher doping level (1.4 eV) is reported by increasing the Li coverage with the emergence of flat bands.[12] However, several questions remain open. How does Li penetrate the top graphene layer, the buffer layer and finally reach the SiC substrate? Is this a sequential process with different intercalation steps? How do the charge states and the Coulomb interactions of Li ions influence the intercalation mechanism, or *vice versa*? More importantly, what are the transport properties of the resulting quasi-free graphene? Here, we address some of these questions.

Department of Materials, ETH Zurich, 8093 Zurich, Switzerland.
E-mail: sebastian.stepanow@mat.ethz.ch; Fax: +4144 633 11 91;
Tel: +41 44 633 07 41

†Electronic supplementary information (ESI) available: Detailed characterizations of Li intercalation, suppressing bulk conduction in Au-contacted epitaxial graphene on SiC. See DOI: https://doi.org/10.1039/d3nr03070a

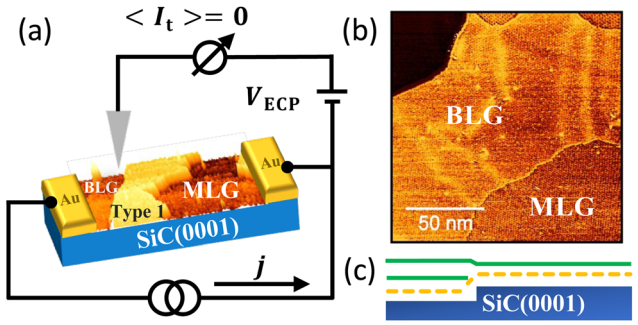

Fig. 1 (a) Schematic of the scanning tunneling potentiometry setup. An external current source applies a current density j = 4 A m^{-1} through two Au contacts deposited on epitaxial graphene. An STM tip is brought a few Angstroms away from the surface and measures the tunneling current I_t. An extra voltage V_{ECP} is applied to the graphene simultaneously and considered as the local ECP if V_{ECP} can zero the tunneling current. (b) 150 × 150 nm STM image of graphene/SiC with a mixture of monolayer and bilayer graphene. The separation between BLG and MLG is visible (image conditions: V_{bias} = 50 mV, I_t = 500 pA). (c) Sketch of the structural transition of a typical MLG/BLG interface, where the yellow dashed lines refer to the buffer layer and the green solid lines represent graphene layers. The small apparent height difference between MLG and BLG originates from a step in the SiC substrate beneath BLG.

Recently, the development of scanning tunneling potentiometry (STP) enabled local electron transport imaging around nanoscopic objects of interest,[16–22] correlating the local electrochemical potential (ECP) with the morphological features as sketched Fig. 1(a). Here, we perform STM and STP to study the Li intercalation processes and their electron transport properties for epitaxial graphene on a SiC(0001) substrate. Two distinct phases of Li intercalated graphene are found and denoted as Type 0 and Type 1. The experiments yield insight into the kinetic processes during the intercalation. The electronic properties of these phases are analyzed using STS. Further, STP measurements at 91 K precisely determine their local electron transport properties. Based on the ECP data, we show that the Type 1 phase reduces the sheet resistance of pristine MLG by 56% and is also more conductive compared to pristine BLG, whereas Type 0 induces only a local potential dip. By discussing the differences in ECP profiles between the two phases, we point out the importance of Li charge transfer for graphene functionalization.

2. Experimental methods

Epitaxial graphene is grown on a SiC-6H(0001) semi-insulating substrate (thickness 330 μm, resistivity >1 × 10^5 Ω cm) by direct current heating in ultra-high vacuum. The sample quality was checked using Raman spectroscopy.[23] Then, 50 nm thick Au contacts are *ex situ* deposited onto the SiC wafer with a Kapton mask protecting the graphene surface. After being reinserted into the UHV chamber, the sample is degassed at around 200 °C for one hour to remove any adsorbates. This results in a clean graphene surface as shown in Fig. 1(b). Li is evaporated *in situ* from a commercial Li dispenser (SAES Getters) on the Au-contacted sample held at 300 K. The sample is then transferred in vacuum to the STM chamber and scanned with an electrochemically etched W tip in the constant current mode. The topographic inspections of the Li-intercalated graphene are performed at 300 K using a four-contact STM from RHK Technology at a base pressure of 1 × 10^{-10} mbar. The sample investigated in this work consists of a mixture of MLG and BLG, exhibiting MLG/BLG interfaces as shown in Fig. 1(b), together with the common SiC triple steps in epitaxial graphene. Fig. 1(c) shows a cross-section sketch across an on-terrace MLG/BLG interface. The dashed yellow line and the green lines represent the buffer layer and the graphene layers, respectively. One missing SiC layer (250 pm) beneath the BLG region accounts for a lower step height (80 pm) compared to the graphene layer thickness (330 pm).

3. Results and discussion

After deposition, Li clusters appear in the MLG regions as shown in Fig. 2(a). The topographic height of the cluster is roughly 150 pm as indicated by the line profile in Fig. 2(d). The periodic superstructure in these regions is due to the modulation of the $6\sqrt{3} \times 6\sqrt{3}$ reconstruction of the buffer layer. The graphene lattice in correspondence to the clusters is strongly distorted relative to pristine MLG (inset), with an apparent local strain reading up to 18% as deduced from the STM images. Raman measurements, however, do not provide evidence for such a strained state of this phase. Raman spectroscopy is performed *ex situ* on micron-wide sample areas, which makes it difficult to confirm the presence of transient local strain.[23] The intercalated Li atoms in this phase are mobile as evidenced by the changing shape and fuzzy edges of the patches at 300 K, which sparsely occupy only the MLG regions. The Li clusters here are irregular shapes with linear dimensions of 20–40 nm. Further experiments and discussions (see below) suggest that the Li atoms are trapped between MLG and buffer layer and remain unbounded (Fig. 2(g)). This phase, which we refer to as Type 0, has not been reported before and allows it to be a precursor to a more stable phase.

Over a timescale of two days, we observe a transition to a new phase, denoted as Type 1 in Fig. 2(b), which has sharper interfaces and a different height (~250 pm) as indicated by Fig. 2(e). The transition from Type 0 to Type 1 occurs gradually over time, as shown by a continuous series of STM images.[23] Type 1 first saturates the MLG/BLG interface completely and then grows inwards beneath the MLG while the BLG region remains unchanged. The atomically-resolved STM image of Type 1 shows a flat topography from the inset in Fig. 2(b) and is similar to the previously reported phase of Li intercalated MLG.[14,15] The dips in the topography are assigned to missing Li atoms beneath the buffer layer. Previous STM, XPS, and LEED measurements indicate that Li atoms directly bond with Si atoms in Type 1 resulting in the complete detachment of the buffer layer.[13,14] Therefore, Type 1 corresponds to the

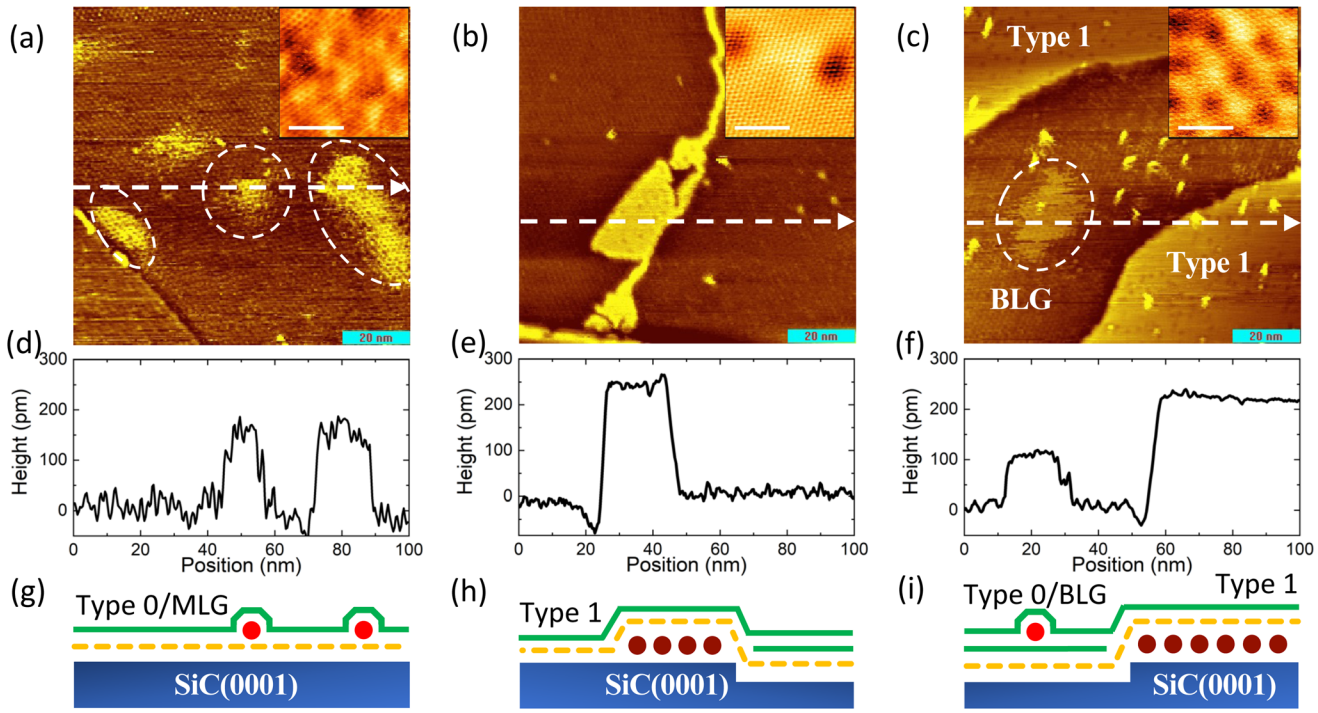

Fig. 2 (a–c) 100 × 100 nm STM images of Li-intercalated graphene around MLG/BLG interfaces at 300 K as a function of Li coverage. (a) Scattered clusters show up immediately after Li deposition as indicated by dashed white circles. The height profile across these clusters is shown in (d) by a white dashed line. These clusters are mobile beneath MLG and eventually nucleate at the MLG/BLG interface in (b) usually within 2 days in UHV. The topographic height changes to 250 pm as shown in the line profile (e). It is considered that Li now bonds with Si atoms and ionizes as sketched in (h). By further increasing the Li coverage, the MLG region is first completely occupied while the mobile clusters show up now in the BLG region in (c) as marked by a dashed circle. The topographic profile across the interface shows a lower height in (f). Li immediately penetrates the top MLG as shown by the regular graphene lattice observed in the insets of the three intercalated phases with a scale bar of 2 nm. The assumed positions of the Li atoms are shown in (g–i). The Li atoms bound to the SiC are shown in dark red to highlight the different bonding with respect to Li bound between the graphene layers which are shown in light red (image conditions: V_{bias} = 50 mV for three insets and (b), V_{bias} = 500 mV for (a and c), I_t = 500 pA for all scans).

quasi-free BLG as sketched in Fig. 2(h), where the Li atoms bind with the SiC substrate and are ionized. The Type 1 phase is stable up to a temperature of 300 °C.[23]

By increasing further the Li coverage, we observe the coexistences of Type 0 and Type 1 phases. As shown in Fig. 2(c) and a line profile in Fig. 2(f), Type 0-like clusters also populate the BLG area. The presence of the $6\sqrt{3} \times 6\sqrt{3}$ reconstruction (inset) suggests that these clusters are intercalated beneath the top graphene layer, similar to the Type 0 clusters observed beneath MLG (Type 0/MLG), as sketched in Fig. 2(i). These clusters are stable over one week, even though their shapes keep changing. However, the Type 0 phase is thermally unstable and removed completely from both MLG and BLG regions by moderate heating up to 120 °C, as shown in Fig. S1(e).†[23]

Based on the STM observations of the Type 0 and Type 1 phase, the phase transition is attributed to a change of Li position beneath MLG as indicated by Fig. 2(g) and (h). Li first penetrates the top graphene layer right after landing on the surface, as proven by STM imaging of the Type 0 phase following Li deposition. Li cannot readily penetrate through a perfect honeycomb lattice but the energy barrier is much reduced when the lattice is stretched or has topological defects like heptagons or octagons.[24] Therefore, the structural defects in the graphene sheets likely promotes intercalation. Moreover, theoretical work shows that Li atoms are more stable between graphene layers rather than on the top graphene layer.[25] Calculations also reveal that Li atoms prefer to bind to the buffer layer/SiC interface rather than intercalating between carbon layers.[26] The Li penetration barrier through the buffer layer is much lower than the one for perfect monolayer graphene,[24] which facilitates intercalation. Despite the homogeneous Li deposition on the surface, Type 0 clusters are initially only found in MLG regions with BLG areas unchanged. The avoidance of BLG intercalation, which has also been observed in Na[27,28] and Mn[29] intercalation, possibly originates from variances in Li diffusion barrier[25,30,30] and adsorption energy[24] on the buffer layer beneath MLG and the buried MLG under BLG, owing to their distinct chemical and structural characteristics.[24,31] While Type 0 clusters diffuse only within MLG regions, reflections at the MLG/BLG interfaces lead to increased proximity to these steps, which initiates Li penetration and phase transition within MLG regions. Type 0 clusters in the BLG area appear after the complete occu-

pation of Type 1 at the MLG/BLG interfaces, hindering diffusion into the MLG region. This signifies that Li prefers to penetrate and diffuse within MLG areas than to intercalate directly below the buffer layer of the BLG region.

To probe the electronic properties of the Li-intercalated phases, STS measurements are performed locally at 300 K. Even with a strong thermal broadening in the spectra, we resolve a local minimum in the dI/dV current, which indicates the position of the Dirac point of graphene. The measurements shown in Fig. 3(a) reveal n-doping levels of 0.5 eV and 0.4 eV for MLG and BLG, respectively, indicating slightly higher doping compared to other reports of 0.42 eV (MLG) and 0.3 eV (BLG).[5] The complete detachment of the buffer layer in Type 1 results in a much higher n-doping level of around 0.8 eV. This agrees with previous STM and ARPES measurements.[12,13,15] Surprisingly, the intermediate Type 0 on both MLG and BLG shows weaker n-doping levels of 0.7 eV and 0.5 eV, respectively, as shown in Fig. 3(b). The strong n-doping in Type 1 is attributed to the ionic nature of Li, which donates one electron to break the Si–C bond.[13,32] If the Li charge state is also the same for Type 0, the doping level of Type 0 should be even stronger due to a reduced screening effect from the buffer layer and closer distance to the topmost graphene as found in a theoretical study.[33] The STS results imply that Li atoms do not bond with the buffer layer or MLG or do not donate a full electron in the Type 0 phase. The differences in Li charge transfer, as predicted theoretically, strongly depend on the Li positions beneath the top graphene layer.[34] The majority of Li charge is transferred to the SiC substrate in Type 1, whereas the charge transfers equally between the buffer layer and MLG in Type 0. Local doping, therefore, varies between the two phases. Theoretical predictions further show that the accumulated charge in the Li-adsorbed graphene depends on the Li concentration.[35] The concentration differences between Type 0 and Type 1 can be directly observed by monitoring transitions in closed MLG regions, as depicted in Fig. S2.† [23] The resulting analysis shows that Type 1 has a Li concentration that is roughly 1.35 times higher than that of Type 0.

The different electron doping levels of graphene are expected to induce a change in the sheet resistance. In order to prove this point, the local transport properties of Li-intercalated graphene are investigated using STP at 91 K to inhibit SiC bulk conduction. The device geometry is drawn in Fig. 1(a). A current density of 4 A m^{-1} is injected into the graphene surface and induces a spatially-dependent electrostatic potential. Using STP, the ECP profiles are measured simultaneously with the surface topography, such that local scattering at defects and interfaces can be imaged. The local sheet resistance is extracted from the ECP maps by fitting the slope parallel to the current direction. Before examining the intercalation of Li, the sheet resistance of pristine MLG and BLG is evaluated. This is done by scanning clean MLG and BLG regions and mapping the ECP over 20 sites on the epitaxial graphene surface. The averaged sheet resistance for MLG and BLG are 677 ± 122 Ω and 545 ± 75 Ω, respectively. These values agree roughly with previous STP measurements on epitaxial graphene.[17,36] The relatively large spread results from the inhomogeneity of the SiC substrate or the local cleanness of the MLG and BLG, which cannot be perfectly controlled during growth.

In Fig. 4(a), an isolated Type 0 cluster with a diameter of 10 nm is imaged on an otherwise clean MLG area. Upon cooling down to 91 K, the size of the Type 0 region shrinks compared to 300 K, which reflects the mobility of this phase and an increased number of nucleation sites at low temperature. The ECP map for the exact same area is shown in Fig. 4(b). To better visualize the local potential modulations,

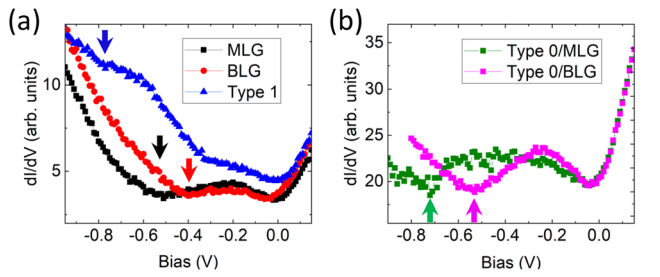

Fig. 3 (a) dI/dV spectra taken on pristine MLG, BLG, and the Type 1 Li-intercalated phase beneath MLG. The arrows indicate the original n-doping of MLG and BLG from the SiC substrate and stronger n-doping induced by the Type 1 intercalation. (b) dI/dV spectra of Type 0 Li-intercalated phase on MLG and BLG. The arrows indicate the position of the Dirac point. The dI/dV measurements are performed at 300 K with a bias modulation frequency of 4.425 kHz and an amplitude of 30 mV.

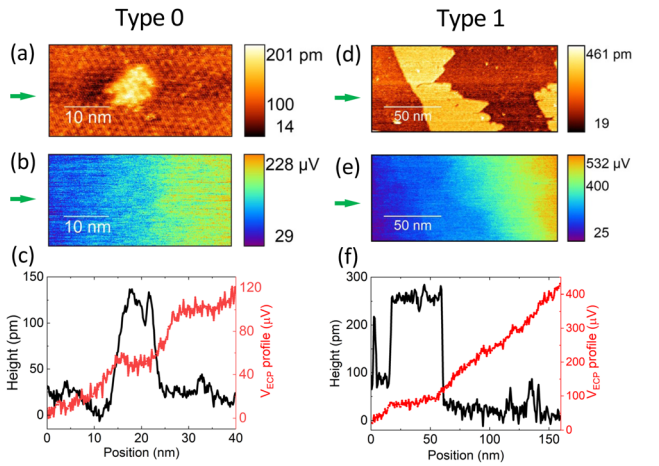

Fig. 4 STP measurements of (a) an isolated Type 0/MLG cluster and (d) a wide stripe of Type 1 phase at a MLG/BLG interface at 91 K. (b) and (e) are the simultaneously obtained ECP maps from the exact same area in (a) and (d), respectively. A current is injected from the right side of the sample, resulting in an increasing ECP = eV_{ECP} from left to right. The green arrows indicate the position where the 5-line averaged profiles are extracted both in topographic and ECP maps. The corresponding profiles are plotted together in (c) for Type 0/MLG and (f) for the Type 1 strip. Image conditions: V_{bias} = 50 mV, I_t = 500 pA, j = 4 A m^{-1}.

5-lines averaged profiles are extracted from both topographic and ECP maps at the positions marked by green arrows Fig. 4 (a and b) and plotted together in Fig. 4(c). In general, the ECP increases in the direction antiparallel to the current, as expected. However, in correspondence of the Li cluster, a local dip is observed in the ECP profile. The sheet resistance in the Type 0 phase cannot be simply extracted due to the changing ECP slopes within the small cluster. However, the dip is consistent with a localized increase of the carrier density. This is further confirmed by STS, which shows extra n-doping of the Type 0 phase compared to pristine MLG.[24,35] The ECP dip is attributed to the local electron accumulation from the charge transfer, inducing charge screening and scattering near its boundaries. Due to the small size of the Type 0 clusters, these edge effects dominate and the sheet resistance cannot be directly measured.

STP measurements on the Type 1 phase show a clear slope change in the ECP map. Fig. 4(d) reports the topographic map of a Type 1 stripe, where the left boundary represents the BLG/Type 1 interface and the right curved boundary marks the Type 1/MLG interface. The corresponding ECP map is given in Fig. 4(e) with the 5-lines averaged profiles shown in Fig. 4(f). The ECP profile changes between Type 1 and MLG, which corresponds to a significant difference of sheet resistance. To further confirm the doping effect, 7 more sites, and 40 ECP profiles are measured and analyzed. The averaged sheet resistance for the Type 1 phase is 293 ± 41 Ω. Compared to MLG, the Li intercalation has reduced the sheet resistance by 56%, which is approximately half the sheet resistance of pristine BLG. Using the Drude model and a two-dimensional electron gas approximation, the relationship between the sheet resistance ρ and mean free path l for the BLG can be described as $\rho l = 12.9\ k\Omega/k_F$ where k_F is the Fermi wave vector of BLG. Based on the k_F value measured in ref. 4, 12 and 37 and a quadratic energy dispersion in BLG, l for the pristine BLG and the Type 1 is estimated to be 32 nm and 45 nm, respectively. An increase of 13 nm is revealed due to Li intercalation, even in the presence of increased carrier densities and charged interfaces.

4. Conclusions

In conclusion, Li intercalation on monolayer and bilayer graphene grown on SiC(0001) revealed two intercalation phases: Type 0 (mobile) and Type 1 (stable). Type 0/MLG only occupies the MLG regions and transforms into Type 1 at MLG/BLG interfaces, whereas Type 0/BLG appears only after the closure of MLG/BLG interfaces due to Type 1 growth. We observe local graphene lattice distortions (up to 18%) on Type 0/MLG but not on Type 1 or Type 0/BLG, which deviates from the previously observed $(\sqrt{3}\times\sqrt{3})R30°$ superstructure.[13] The different Li charge transfer mechanisms between Type 0 and Type 1 lead to distinct doping effects. Type 1 significantly reduces the sheet resistance of MLG by 56%, while Type 0 only causes local electron scattering. The processes of Li intercalation in epitaxial graphene have been extensively studied theoretically.[24–26,30,34,35] Here we provide a detailed analysis on how adsorption, diffusion, and intercalation affect Li charge transfer and the local carrier density of graphene based on STM and STP data. By correlating structural observation with the electron transport properties directly, our findings highlight the critical role of different intercalation processes in modifying the graphene properties. Future work could examine the functionalization of graphene by intercalation with different p and n dopants. Furthermore, nanoscopic p–n junctions could be constructed on graphene, where quantum electrodynamics phenomena such as Klein tunneling effect can be directly investigated.[38]

Author contributions

W.H. performed the STM and STP experiments, including data analysis and visualization and wrote the manuscript. J.S. and M.P.C. performed the Raman experiments and analyzed the data. S.S. supervised the Raman, STM and STP measurements. P.G. and S.S. conceptualized the project and contributed to the writing of the manuscript.

Conflicts of interest

There are no conflicts to declare.

Acknowledgements

We acknowledge funding from the Swiss National Science Foundation, Project No. 200021_163225 and 200020_207478. H. W. was supported by the China Scholarship Council (CSC) under Grant No. 201806340092.

References

1 Y.-M. Lin, C. Dimitrakopoulos, K. A. Jenkins, D. B. Farmer, H.-Y. Chiu, A. Grill and P. Avouris, *Science*, 2010, **327**, 662–662.
2 Q. Wang, W. Zhang, L. Wang, K. He, X. Ma and Q. Xue, *J. Phys.: Condens. Matter*, 2013, **25**, 095002.
3 P. Landois, T. Wang, A. Nachawaty, M. Bayle, J.-M. Decams, W. Desrat, A.-A. Zahab, B. Jouault, M. Paillet and S. Contreras, *Phys. Chem. Chem. Phys.*, 2017, **19**, 15833–15841.
4 P. Mallet, I. Brihuega, S. Bose, M. M. Ugeda, J. M. Gomez-Rodriguez, K. Kern and J.-Y. Veuillen, *Phys. Rev. B: Condens. Matter Mater. Phys.*, 2012, **86**, 045444.
5 U. Starke, S. Forti, K. Emtsev and C. Coletti, *MRS Bull.*, 2012, **37**, 1177–1186.
6 D. Marchenko, A. Varykhalov, J. Sánchez-Barriga, T. Seyller and O. Rader, *Appl. Phys. Lett.*, 2016, **108**, 172405.

7 Y. Zhang, H. Zhang, Y. Cai, J. Song and P. He, *Nanotechnology*, 2017, **28**, 075701.
8 L. Daukiya, M. N. Nair, M. Cranney, F. Vonau, S. Hajjar-Garreau, D. Aubel and L. Simon, *Prog. Surf. Sci.*, 2019, **94**, 1–20.
9 I. Deretzis and A. La Magna, *Phys. Rev. B: Condens. Matter Mater. Phys.*, 2011, **84**, 235426.
10 G. Profeta, M. Calandra and F. Mauri, *Nat. Phys.*, 2012, **8**, 131–134.
11 B. Ludbrook, G. Levy, P. Nigge, M. Zonno, M. Schneider, D. Dvorak, C. Veenstra, S. Zhdanovich, D. Wong, P. Dosanjh, *et al.*, *Proc. Natl. Acad. Sci. U. S. A.*, 2015, **112**, 11795–11799.
12 C. Bao, H. Zhang, X. Wu, S. Zhou, Q. Li, P. Yu, J. Li, W. Duan and S. Zhou, *Phys. Rev. B*, 2022, **105**, L161106.
13 C. Virojanadara, S. Watcharinyanon, A. Zakharov and L. I. Johansson, *Phys. Rev. B: Condens. Matter Mater. Phys.*, 2010, **82**, 205402.
14 S. Fiori, Y. Murata, S. Veronesi, A. Rossi, C. Coletti and S. Heun, *Phys. Rev. B*, 2017, **96**, 125429.
15 M. Omidian, N. Néel, E. Manske, J. Pezoldt, Y. Lei and J. Kröger, *Surf. Sci.*, 2020, **699**, 121638.
16 A. Bannani, C. Bobisch and R. Möller, *Rev. Sci. Instrum.*, 2008, **79**, 083704.
17 S.-H. Ji, J. Hannon, R. Tromp, V. Perebeinos, J. Tersoff and F. Ross, *Nat. Mater.*, 2012, **11**, 114–119.
18 K. W. Clark, X.-G. Zhang, I. V. Vlassiouk, G. He, R. M. Feenstra and A.-P. Li, *ACS Nano*, 2013, **7**, 7956–7966.
19 P. Willke, M. Schneider and M. Wenderoth, *Ann. Phys.*, 2017, **529**, 1700003.
20 F. Lüpke, M. Eschbach, T. Heider, M. Lanius, P. Schüffelgen, D. Rosenbach, N. Von Den Driesch, V. Cherepanov, G. Mussler, L. Plucinski, *et al.*, *Nat. Commun.*, 2017, **8**, 15704.
21 T. Marković, W. Huang, P. Gambardella and S. Stepanow, *Rev. Sci. Instrum.*, 2021, **92**, 103707.
22 Z. J. Krebs, W. A. Behn, S. Li, K. J. Smith, K. Watanabe, T. Taniguchi, A. Levchenko and V. W. Brar, *Science*, 2023, **379**, 671–676.
23 See ESI† for additional information.
24 Y. Li, G. Zhou, J. Li, J. Wu, B.-L. Gu and W. Duan, *J. Phys. Chem. C*, 2011, **115**, 23992–23997.
25 I. Shtepliuk and R. Yakimova, *Appl. Surf. Sci.*, 2021, **568**, 150988.
26 T. Bijoy and P. Murugan, *J. Phys. Chem. C*, 2019, **123**, 10738–10745.
27 A. Sandin, T. Jayasekera, J. Rowe, K. W. Kim, M. B. Nardelli and D. B. Dougherty, *Phys. Rev. B: Condens. Matter Mater. Phys.*, 2012, **85**, 125410.
28 S.-M. Choi and S.-H. Jhi, *Appl. Phys. Lett.*, 2009, **94**, 153108.
29 T. Gao, Y. Gao, C. Chang, Y. Chen, M. Liu, S. Xie, K. He, X. Ma, Y. Zhang and Z. Liu, *ACS Nano*, 2012, **6**, 6562–6568.
30 K. Persson, Y. Hinuma, Y. S. Meng, A. Van der Ven and G. Ceder, *Phys. Rev. B: Condens. Matter Mater. Phys.*, 2010, **82**, 125416.
31 S. Kim, J. Ihm, H. J. Choi and Y.-W. Son, *Phys. Rev. Lett.*, 2008, **100**, 176802.
32 F. Bisti, G. Profeta, H. Vita, M. Donarelli, F. Perrozzi, P. Sheverdyaeva, P. Moras, K. Horn and L. Ottaviano, *Phys. Rev. B: Condens. Matter Mater. Phys.*, 2015, **91**, 245411.
33 T. P. Kaloni, Y. Cheng, M. U. Kahaly and U. Schwingenschlögl, *Chem. Phys. Lett.*, 2012, **534**, 29–33.
34 N. M. Caffrey, L. I. Johansson, C. Xia, R. Armiento, I. A. Abrikosov and C. Jacobi, *Phys. Rev. B*, 2016, **93**, 195421.
35 Y. Liu, Y. M. Wang, B. I. Yakobson and B. C. Wood, *Phys. Rev. Lett.*, 2014, **113**, 028304.
36 P. Willke, T. Kotzott, T. Pruschke and M. Wenderoth, *Nat. Commun.*, 2017, **8**, 15283.
37 T. Ohta, A. Bostwick, J. L. McChesney, T. Seyller, K. Horn and E. Rotenberg, *Phys. Rev. Lett.*, 2007, **98**, 206802.
38 M. Katsnelson, K. Novoselov and A. Geim, *Nat. Phys.*, 2006, **2**, 620–625.